The Astronomical Journal, 152:73 (14pp), 2016 September doi:10.3847/0004-6256/152/3/73

STELLAR NUCLEI AND INNER POLAR DISKS IN LENTICULAR GALAXIES

Olga K. Sil'chenko
Sternberg Astronomical Institute, M.V. Lomonosov Moscow State University, Moscow, 119992 Russia; olga@sai.msu.su
Isaac Newton Institute, Chile, Moscow Branch
Received 2015 August 18; revised 2016 June 10; accepted 2016 June 21; published 2016 September 6

ABSTRACT

I analyze statistics of the stellar population properties for stellar nuclei and bulges of nearby lenticular galaxies in different environments by using panoramic spectral data of the integral-field spectrograph SAURON retrieved from the open archive of the Isaac Newton Group. I also estimate the fraction of nearby lenticular galaxies having inner polar gaseous disks by exploring the volume-limited sample of early-type galaxies of the ATLAS-3D survey. By inspecting the two-dimensional velocity fields of the stellar and gaseous components with the running tilted-ring technique, I have found seven new cases of inner polar disks. Together with those, the frequency of inner polar disks in nearby S0 galaxies reaches 10%, which is much higher than the frequency of large-scale polar rings. Interestingly, the properties of the nuclear stellar populations in the inner polar ring hosts are statistically the same as those in the whole S0 sample, implying similar histories of multiple gas-accretion events from various directions.

Key words: galaxies: elliptical and lenticular, cD – galaxies: ISM – galaxies: kinematics and dynamics – galaxies: stellar content

1. INTRODUCTION

Outer gas accretion is now recognized as a main driver of disk galaxy evolution: neither the prolonged star formation observed in disks of spiral galaxies nor the observed chemical abundances in their stars can be explained without a continuous gas supply from outside. Indeed, the gas depletion time in nearby spirals is found to concentrate tightly around the value of only 2–3 Gyr (Bigiel et al. 2011), while the solar abundance ratios of the disk stellar populations imply a duration of continuous star formation of more than 3 Gyr. The "G-dwarf paradox" and the absence of the age–metallicity correlation in the thin stellar disk of our own Galaxy (Chiosi 1980; Tosi 1988) as well as the lowered effective oxygen yield in the disks of other spiral galaxies (Pilyugin et al. 2004; Dalcanton 2007) require such accretion. However, direct observational findings of outer-gas accretion signatures are rather rare despite the fact we expect these events to happen daily. Perhaps it would be easier to search for consequences of outer gas accretion in early-type disk galaxies, namely in S0s, where the gas of the galaxies, usually absent, does not prevent rather long-lived kinematical misalignments between the stellar disks and the accreted gaseous subsystems.

One of the brightest phenomena betraying the outer-gas accretion events are *inner* polar rings or disks of ionized gas that are embedded deeply in the bulge-dominated area. The presence of some minor species with a decoupled momentum can be explained only by such accretion. The first finding of an inner polar disk was noted by Bettoni et al. (1990) in the SB0 galaxy NGC 2217 from the multiple long-slit cross sections of this barred galaxy; the complex gas kinematics was explained by a strong warp of the gas rotation plane in the center of the galaxy, such that the central gas rotation proceeded in the plane orthogonal to the stellar rotation plane and also to the bar major axis. After the rise of the era of integral-field spectroscopy, inner polar disks were also found in many unbarred galaxies, in particular in Sb galaxy NGC 2841 (Sil'chenko et al. 1997), in Sb galaxy NGC 7742 (Sil'chenko & Moiseev 2006), and in isolated Sa galaxy NGC 7217 (Sil'chenko & Afanasiev 2000). They were detected exclusively through the kinematical analysis: the integral-field spectroscopy allowed determination of spatial orientations of the rotation axes both for the stellar and ionized-gas components, and if these rotation axes appeared to be mutually orthogonal, the presence of the inner polar disk could be claimed. Sometimes inner polar rings of ionized gas could be seen as dust lanes aligned along the minor axes of the isophotes: in such a way we found eight inner polar disks in lenticular galaxies whose high-resolution images were provided by the *Hubble Space Telescope* (Sil'chenko & Afanasiev 2004). The first list of 17 galaxies that were claimed to possess inner polar disks was presented by Corsini et al. (2003).

Now a few dozen inner polar gaseous disks are already known, and the time to examine their statistics has come. Moiseev (2012) has assembled a list of 47 inner polar disks reported by various authors before 2012 and has presented some general properties of the inner polar disks and their host galaxies. First, these disks are indeed polar: though all the gaseous rings whose rotation axes are inclined to the stellar rotation axes by more than 50° have been considered, the distribution of the mutual inclinations peaks strongly at 90°. Second, they can be found mostly in early-type galaxies: more than half of all known inner polar disks belong to (mostly) lenticular and elliptical galaxies; however, a few belonging to very late-type dwarfs are also known. The typical radii of the inner polar disks range from 0.2 to 2.0 kpc; the outer boundary is quite real, revealing the relation of the inner polar disks to bulge-dominated areas, while the inner limit results from the finite spatial resolution of ground-based integral-field spectroscopy.

However, the review by Moiseev (2012) operated with a very heterogeneous sample of casual observational findings. A particular question remains unanswered: what is the frequency of inner polar disks/rings in the whole ensemble of nearby lenticular galaxies? The answer would help to specify the geometry of the outer-gas accretion and so to identify its

sources. In the case of isotropic accretion, we would be able to estimate the theoretical fraction of inner polar rings by taking into account their dynamical evolution—precession and sinking to the main symmetry planes. If the theoretical estimates diverge from the observational statistics, it may be a hint to an anisotropic accretion-source distribution, for example, accretion from a single neighbor galaxy or multiple minor mergers from the satellite plane. I have undertaken a further attempt to increase the number of the known inner polar disks by using the possibility provided by the integral-field spectral data for a sample of early-type galaxies that have been obtained with the Integral-Field Unit Spectroscopic Areal Unit for Research on Optical Nebulae (IFU SAURON; Bacon et al. 2001) in the frame of the ATLAS-3D survey (Cappellari et al. 2011a). The ATLAS-3D sample was volume-limited and complete above the absolute magnitude of $M_K = -21.5$, so I hoped to estimate reliably the frequency of inner polar disks in nearby lenticular galaxies from these data. The data of the ATLAS-3D survey are freely available from the Isaac Newton Group (ING) Archive (CASU Astronomical Data Centre at the Institute of Astronomy, Cambridge) after the end of the proprietary period, and I have retrieved the raw data for about 150 lenticular galaxies to analyze the kinematics of the stellar and ionized-gas components in the central parts of these galaxies and to search for new cases of inner polar disks.

2. THE DATA OF THE ATLAS-3D SURVEY

The integral-field spectrograph SAURON was operating at the 4.2 m William Herschel Telescope belonging to the ING of telescopes on La Palma. It worked in "TIGER mode," giving about 1500 spectra simultaneously, each for a $0\farcs94 \times 0\farcs94$ square element ("spaxel") from a (central) part of a galaxy. A total set of spectra covers an area of $41'' \times 33''$. The spectral range of the unit is rather narrow, 4800–5350 Å, and its spectral resolution has been fixed since 2007 at about 4.3 Å.

There were two surveys of nearby early-type galaxies with SAURON. The first one, which started in 1999 and finished in 2004, involved 72 galaxies, among those 48 early-type ones and 24 spirals (de Zeeuw et al. 2002). The second one undertaken in 2007–2008 added more early-type galaxies, including dwarfs, to complete the volume-limited ($D < 42$ Mpc) sample (Cappellari et al. 2011a). The total sample of early-type galaxies investigated in these two surveys includes 260 objects, and 200 of them are lenticular galaxies. For my analysis I have selected a subsample of 143 S0 galaxies that were observed in 2007–2008, because the design of SAURON was successfully modified just before 2007. Due to a new volume-phase grating, the last data show much less shift of the spectral range over the field of view, and the problems of the first SAURON survey with the absorption lines Hβ and Fe Iλ5270, which are at the edges of the spectral range exposed (de Zeeuw et al. 2002; Kuntschner et al. 2006), are now overcome.

3. ANALYSIS OF THE DATA

The raw data, both scientific frames and calibration frames, have been retrieved for these 143 S0 galaxies from the ING Archive and reduced in a manner that is described in my earlier paper (Sil'chenko 2005). The spectra of a few dozen stars, mostly F–K giants from the Lick standard list (Worthey et al. 1994), have also been reduced and used, first, for cross-correlation with the galactic spectra, to derive stellar line-of-sight (LOS) velocity fields and stellar velocity dispersion fields, and second, to establish a system of the Lick indices (Worthey et al. 1994) used for diagnostics of the stellar population properties. The Lick index system was checked for every observational run separately; an example of such a calibration for the second half of the 2007 April observational run can be seen in Figure 1. The intrinsic scatter of the stars around the calibration lines is about 0.2–0.3 Å, which is consistent with the declared accuracy of the standard star measurements in Worthey et al. (1994); our internal accuracy of the index measurements estimated from repetitive observations of the same stars is better than 0.05 Å. As one can see, the spectral range of the observations in 2007 was optimal for measuring the indices Hβ, Mgb, and Fe5270; even Fe5335 for the zero redshift is calibrated appropriately, though it cannot be used in galaxies with nonzero redshifts. After subtracting the stellar continuum, I also extracted emission-line spectra, which were used to calculate LOS velocities of the ionized gas by measuring baricenter positions of the strongest emission line in this spectral range, [O III]λ5007 Å.

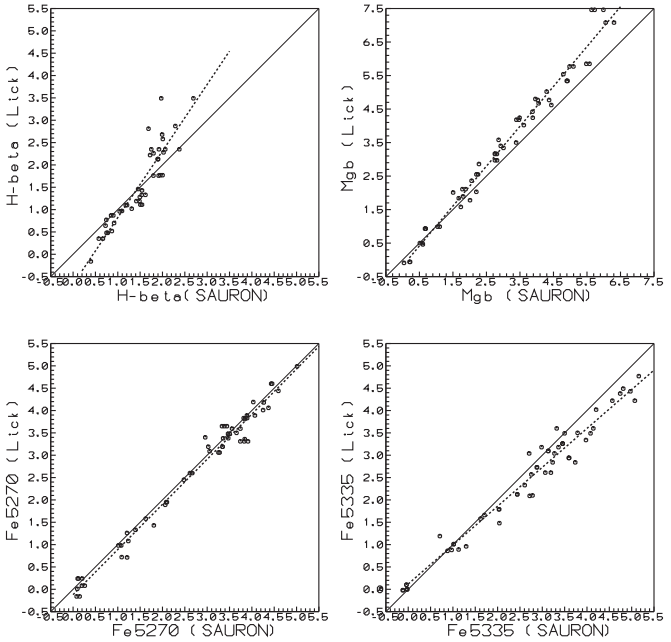

Figure 1. One calibration of the Lick index system using standard stars from the list of Worthey et al. (1994): straightforward index measurements from the SAURON spectra are compared against the standard Lick values. Symbols mark the measurements of individual stars, straight solid lines are equality lines, and dashed lines show the least-squares fit that was used to calibrate the instrumental SAURON measurements onto the standard Lick index system. These particular regressions are obtained for the observational run of 2007 April 19–25.

These LOS velocity maps, both for the stellar (s) and ionized-gas (g) components, have been analyzed in the frame of a tilted-ring approach in a particular modification by Alexei Moiseev (Moiseev et al. 2004 with the DETermination of Kinematics for gAlaxies (DETKA) software). This technique allows us to estimate the parameters of the spatial orientation of the rotation planes for both components, namely, the inclinations of the rotation planes $i_{s,g}$ and the position angles of lines of nodes, $\mathrm{PA}_{s,g}$. After that, the mutual inclinations of the stellar and gaseous rotation planes have been calculated by

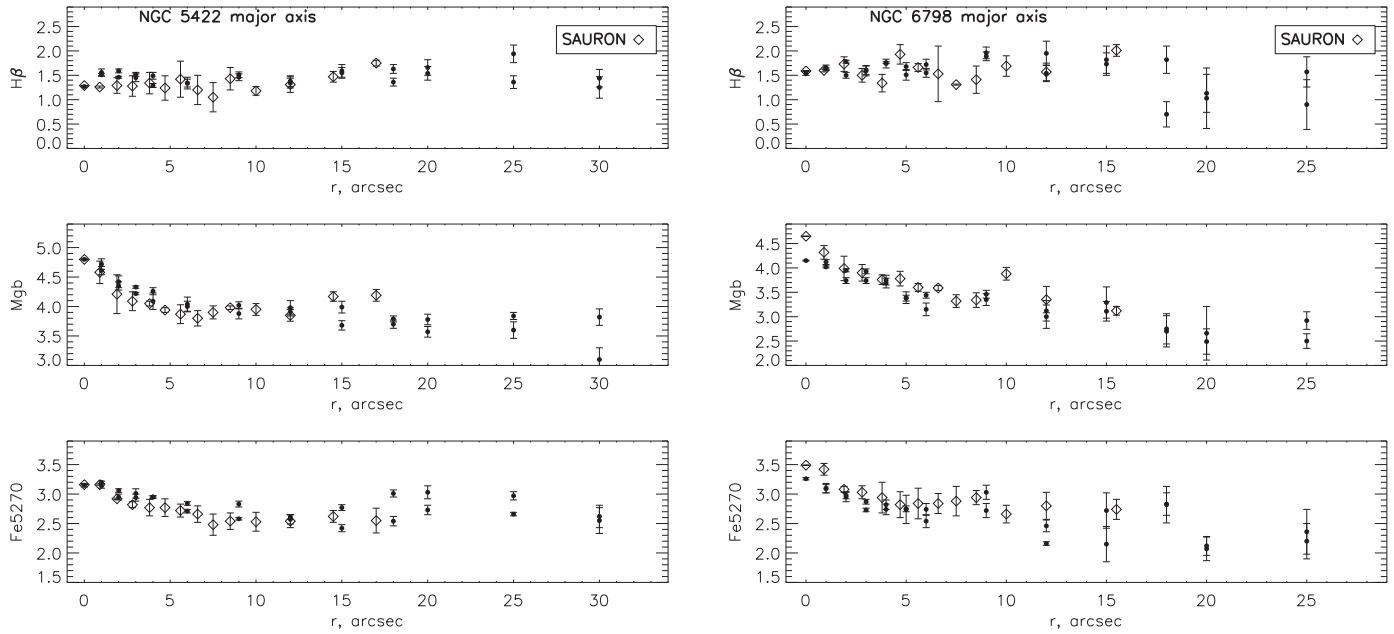

Figure 2. Comparison of the Lick index profiles obtained by using the SAURON data with those observed by us at the Russian 6 m telescope with the long-slit spectrograph SCORPIO. Two halves of our long-slit cross sections symmetric with respect to the nuclei are superimposed, while the SAURON data are averaged in the radius bins.

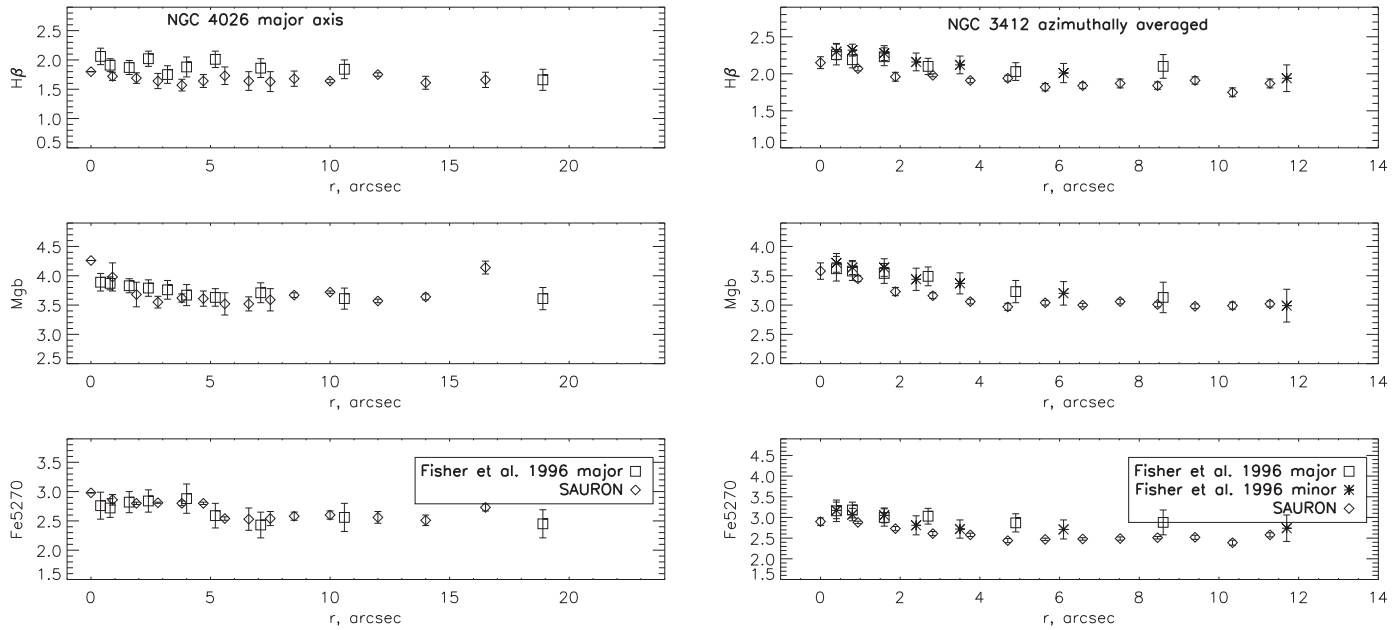

Figure 3. Comparison of the Lick index profiles obtained by using the SAURON data with those observed along the major and minor axes of the galaxies with a long-slit spectrograph by Fisher et al. (1996).

using the following formula (Moiseev 2012):

$$\cos\Delta i = \pm\cos(\mathrm{PA}_s - \mathrm{PA}_g)\sin i_s \sin i_g + \cos i_s \cos i_g.$$

The equation has two solutions because typically we do not know which side of a galactic disk is closer to us. If for the regularly rotating stellar and gaseous components I obtain both possible mutual inclinations $\Delta i > 50°$, I consider the circumnuclear ionized-gas component to be an inner polar disk. Please note that to determine the mutual inclination of two rotation planes, one needs to know not only the kinematical misalignment, $(\mathrm{PA}_s - \mathrm{PA}_g)$, but also the inclinations of the planes to the sky plane, i_s and i_g. Only in the case when both planes are seen nearly edge-on is the term with $(\mathrm{PA}_s - \mathrm{PA}_g)$ dominant; alternatively, if one of the planes is close to face-on, the kinematical misalignment does not take any part in the mutual inclination determination. This is just why I can state that the ATLAS-3D team (Davis et al. 2011; Krajnovic et al. 2011) has not established the presence of inner polar disks in the galaxies of their sample: they have measured only kinematical misalignment $(\mathrm{PA}_s - \mathrm{PA}_g)$ by applying the kinemetry approach, and only the statistics of this misalignment has been considered (Davis et al. 2011); while to determine the intrinsic

Table 1
Lick Indices and SSP-equivalent Parameters for the Nuclei

Galaxy[a]	Eq. Width of [O III] λ5007, Å	Hβ	Mgb	Fe5270	*T*, Gyr	[*Z*/*H*], dex
N448	0.19	1.83	4.42	3.06	4	+0.5
N502	0.12	1.96	4.80	3.40	3	+0.8
N509	0.84	3.37	2.38	2.32	1	+0.4
N516	0.68	2.25	2.90	2.82	2	+0.2
N525	0.24	2.18	3.38	2.53	3	+0.1
N1121	0	1.59	4.98	2.71	14	0.0
N1248	0.29	2.40	3.49	2.84	1.5	+0.5
N1289	0.73	1.92	3.70	2.86	2	+0.4
N1665	0.30	2.31	3.84	3.18	2	+0.7
N2481	0.41	1.55	4.39	3.04	5	+0.4
N2577	0.27	1.48	5.02	2.88	8	+0.3
N2592	0	1.49	5.11	2.82	12	+0.2
N2697	0.52	1.94	3.62	3.13	2	+0.5
N2698	0	1.84	4.93	2.77	5	+0.4
N2824	1.25	1.00	3.36	2.36	11	-0.2
N2852	0.96	1.31	5.20	2.56	5	+0.3
N2859	0.31	1.59	4.73	3.24	5	+0.5
N2880	0.28	2.20	4.08	3.06	2	+0.7
N2950	0.14	2.14	4.66	3.08	2	+0.7
N2962	0.80	1.37	5.23	3.24	4	+0.7
N3098	0.24	1.88	3.16	2.64	5	−0.1
N3182	3.67	1.56	4.88	3.36	3	+0.8
N3230	0.10	1.42	5.04	2.92	12	+0.2
N3245	0.62	0.24	4.73	2.66	15	+0.0
N3248	0.64	2.51	3.78	3.03	1	+1.0
N3301	0.44	2.10	3.45	2.48	3	+0.1
N3400	0.39	2.08	3.65	3.17	2	+0.7
N3412	0.18	2.15	3.58	2.90	2	+0.4
N3457	0.64	2.18	3.24	2.43	2	+0.1
N3458	0	1.59	4.53	2.95	11	+0.2
N3499	0.32	2.18	3.61	3.10	2	+0.5
N3530	0.17	1.79	3.56	2.77	6	0.0
N3595	0.54	1.80	4.28	2.75	3	+0.4
N3599	2.93	1.95	3.37	2.89	2	+0.4
N3607	0.34	1.24	5.01	3.03	12	+0.3
N3610	0.34	2.10	4.32	2.83	2	+0.7
N3613	0	1.70	4.82	2.99	7	+0.4
N3619	1.19	1.49	4.56	3.18	3	+0.7
N3626	0.53	2.76	3.31	2.72	1	+0.8
N3630	0	1.77	4.61	3.22	5	+0.5
N3648	0.81	1.04	5.75	3.18	7	+0.6
N3658	0.10	2.03	4.65	3.47	3	+0.8
N3665	0.28	1.16	4.86	3.26	15	+0.3
N3674	0	1.57	4.94	2.97	10	+0.3
N3694	1.73	0.74	3.36	2.20	12	−0.3
N3757	0.35	1.70	3.65	2.90	5	+0.15
N3796	0.38	2.91	2.68	2.22	1.5	+0.1
N3838	0.17	2.02	3.90	2.68	3.5	+0.2
N3941	0.50	1.90	4.81	3.36	2	+0.8
N3945	0.50	1.45	5.35	3.44	4	+0.8
N4026	0.19	1.80	4.26	2.98	4	+0.3
N4036	1.42	0.16	5.42	2.87	15	+0.2
N4078	0.10	1.69	4.41	2.78	8	+0.15
N4111	0.58	2.11	4.09	2.91	2	+0.7
N4124	0.48	2.84	2.67	2.23	1.5	+0.1
N4143	0.62	0.85	5.60	3.04	15	+0.3
N4179	0.10	2.26	4.63	3.21	2	+0.8
N4191	0.71	1.79	4.32	3.01	2	+0.7
N4215	0.18	2.26	4.07	2.75	2	+0.5
N4233	0.84	1.69	5.30	3.32	3	+1.0
N4249	0.40	2.07	4.00	3.01	2	+0.7
N4251	0.20	2.03	4.15	2.99	3	+0.5

Table 1
(Continued)

Galaxy[a]	Eq. Width of [O III] λ5007, Å	Hβ	Mgb	Fe5270	*T*, Gyr	[*Z*/*H*], dex
N4255	0.40	1.52	4.40	2.77	8	+0.15
N4259	0.38	1.83	4.12	2.80	4	+0.3
N4264	0.26	2.15	4.10	3.20	2	+0.8
N4267	0	1.60	5.09	2.95	9	+0.4
N4281	0.08	1.81	4.92	3.15	4	+0.6
N4324	1.33	1.83	4.00	3.23	5	+0.4
N4340	0.28	2.19	4.11	3.61	2	+1.0
N4342	0	1.42	5.53	2.97	12	+0.4
N4346	0.18	1.96	4.03	3.14	3	+0.5
N4350	0.13	1.37	4.66	3.19	12	+0.3
N4371	0.24	1.69	4.33	3.06	5	+0.4
N4377	0	1.86	4.31	2.77	6	+0.2
N4417	0.15	1.73	4.19	2.95	6	+0.2
N4429	0.38	1.75	4.75	3.04	3	+0.6
N4434	0.17	1.79	4.77	3.14	3	+0.6
N4442	0.35	1.59	5.58	3.35	4	+0.8
N4452	0.29	1.88	3.15	2.69	5	0.0
N4461	0.11	1.95	5.10	3.56	3	+1.0
N4474	0.30	2.13	3.65	2.61	4	+0.1
N4476	0.35	2.40	2.75	2.23	2	−0.05
N4483	0.33	2.08	4.36	2.89	2	+0.7
N4503	0.15	1.92	4.99	3.57	3	+1.0
N4521	0.47	1.38	5.03	3.35	5	+0.5
N4528	0.32	2.13	3.73	2.45	3	+0.2
N4578	0.20	1.87	4.94	2.95	3	+0.7
N4596	0.15	1.37	4.66	3.19	12	+0.3
N4608	0.12	1.74	4.29	2.84	7	+0.2
N4612	0.44	2.77	3.41	3.01	1	+1.0
N4623	0.22	2.15	3.70	2.97	2	+0.5
N4624	0.27	1.58	4.74	3.12	5	+0.4
N4638	0.20	2.15	4.45	3.29	2	+1.0
N4643	0.36	1.97	4.50	3.02	3	+0.7
N4690	0.40	1.78	2.55	3.49	6	0.0
N4710	0.78	−0.27	3.02	2.11	1	+0.8
N4733	0.21	2.51	3.33	3.06	1.5	+0.7
N4753	0.21	1.98	4.23	3.51	3	+0.8
N4754	0.10	1.59	5.21	3.45	5	+0.7
N4762	0.26	0.75	4.90	3.02	3	+0.6
N5103	0.47	1.90	4.24	3.11	3	+0.7
N5342	0.16	1.19	4.96	2.70	15	+0.1
N5353	0.28	0.98	5.53	3.14	15	+0.3
N5355	0.33	5.23	2.26	2.14	1	+0.7
N5358	0.33	2.02	3.46	2.77	3	+0.2
N5422	0.60	1.29	4.80	3.16	7	+0.4
N5473	0	1.89	4.50	3.06	4	+0.4
N5485	0.23	1.61	4.84	2.93	6	+0.4
N5493	0.20	2.06	3.25	2.62	4	0.0
N5507	0.53	1.11	6.04	3.04	9	+0.5
N5574	0.37	3.94	2.48	2.52	1	+0.8
N5611	0.28	1.94	4.03	2.70	4	+0.2
N5631	0.44	1.79	4.74	3.23	3	+0.8
N5687	0.15	1.77	4.85	3.50	4	+0.8
N5770	0.27	2.19	4.15	3.14	2	+0.8
N5839	0.13	1.52	5.02	3.32	6	+0.5
N5854	0.21	2.41	2.98	2.58	2	+0.1
N5864	0.22	1.95	3.80	3.10	3	+0.5
N5869	0	1.70	5.19	3.18	5	+0.5
N6010	0.29	2.09	4.54	3.07	2	+0.7
N6017	1.13	1.83	3.56	2.60	2	+0.4
N6149	1.06	1.63	3.98	2.16	3	+0.1
N6278	0.56	1.06	4.91	3.10	14	+0.2
N6703	0.23	1.58	4.88	3.26	5	+0.5

Table 1
(Continued)

Galaxy[a]	Eq. Width of [O III] λ5007, Å	Hβ	Mgb	Fe5270	T, Gyr	[Z/H], dex
N6798	1.25	1.59	4.65	3.49	2	+1.0
N7693	0.19	4.71	1.89	2.18	1	+0.8
N7710	0.69	1.52	3.43	2.89	5	+0.1
N7743	5.5	2.03	3.30	2.54	1	+1.0
I560	3.17	1.97	2.48	2.22	1	+0.2
I598	0.54	2.65	2.59	2.35	1.7	+0.1
I719	0.39	1.68	3.45	2.77	6	0.0
I782	0.35	2.92	3.11	2.44	1	+0.7
U4551	0.23	1.65	4.16	2.86	8	+0.15
U6062	0.25	1.50	4.45	3.22	8	+0.3
U8876	0.11	1.73	3.98	2.64	9	0.0
U9519	0.38	3.04	2.77	2.36	1	+0.3
P28887	0.43	1.42	4.24	2.32	12	−0.15
P35754	0.78	1.97	3.75	2.32	2	+0.2
P42549	1.31	2.31	3.11	2.84	1	+0.8
P44433	0.34	1.92	4.13	2.76	3	+0.3
P50395	0.39	2.34	3.32	2.54	2	+0.15
P51753	0.88	1.65	3.52	2.59	4	+0.1
P54452	0.39	2.10	3.50	3.25	2	+0.5

Note.
[a] Galaxy ID: N = NGC, U = UGC, I = IC, P = PGC.

orientations of the rotation planes, a full tilted-ring approach is needed. That is done in the present work.

The maps of the Lick indices Hβ, Mgb, and Fe5270 calibrated into the standard Lick system and corrected for the stellar velocity dispersion broadening as described in Sil'chenko (2005) have also been calculated for all the S0s without too-strong emission lines in the centers: EW([O III]λ5007) < 2 Å. If the emission lines were less strong, I rectified the Hβ indices by applying an approach proposed by Trager et al. (2000a): a correction of $\Delta H\beta = 0.6\mathrm{EW}([\mathrm{O\ III}]\lambda5007)$ was added to the measured value of the Hβ index to take into account contamination by ionized-hydrogen emission. As I found earlier by studying a sample of S0 galaxies with spectra in the full optical range (Sil'chenko 2006), under this condition, EW([O III]λ5007) < 2 Å, the Hβ correction for the emission contamination is the same when calculated either through the empirical relation with [O III] or through the Balmer decrement applied to the Hα emission-line measurements. When emission lines are strong, EW([O III]λ5007) > 2 Å, the correction through [O III] works poorly. However, for a few galaxies with rather strong emission lines, we have our own long-slit spectra covering the red spectral range for NGC 3599 (Sil'chenko et al. 2010), for NGC 7743 (Katkov et al. 2011), and for IC 560 (Proshina et al. 2016). This makes it possible to identify the gas excitation mechanism by using the Baldwin–Phillips–Terlevich (BPT) diagrams (Baldwin et al. 1981) and to determine the Hβ correction for the emission through the Hα emission-line equivalent-width estimates by applying a model Balmer decrement suitable for the particular excitation mechanism. If the gas is fully excited by young stars, the model from Burgess (1958) is used, and if LINER- or shock-like excitation is added, we apply the correction $\Delta H\beta \approx 0.25$ EW(Hα emis), the empirical Balmer decrement found by Stasinska & Sodré (2001) for a large sample of disk galaxies that corresponds to the mixed gas excitation.

After obtaining the corrected index maps, for the further analysis of the data, radial profiles of the Lick indices were derived by averaging indices over the rings with the width of one spaxel for the galaxies moderately inclined to the line of sight (with the isophote axis ratio less than 1.5), or by superimposing a digital slit with a width of 2.″5–3″ (a compromise between the spatial resolution defined by the seeing and a necessity of a sufficient signal-to-noise ratio) to derive major-axis index profiles for the strongly inclined galaxies. Since some brighter members of the sample have already been studied concerning their Lick index distributions, I can compare the measurements of the Lick indices from the SAURON data with some well-calibrated long-slit spectral data. Figure 2 shows the comparison of the major-axis index profiles for two galaxies, NGC 5422 and NGC 6798, observed by us earlier with the reducer SCORPIO (Afanasiev & Moiseev 2011) of the Russian 6 m telescope and published elsewhere (Sil'chenko 2013; Katkov et al. 2014b). Figure 3 shows the comparison of two variants of the Lick index profiles derived from the SAURON maps—ones averaged over full-azimuth rings for NGC 3412 and the others cut by the digital slit along the equator (PA = 178°) for the edge-on galaxy NGC 4026—with the long-slit data by Fisher et al. (1996). One can see an overall agreement of the profiles, so I conclude that I have succeeded in measuring the Lick indices in the SAURON data without noticeable systematic shifts.

4. CHARACTERISTICS OF THE NUCLEAR AND BULGE STELLAR POPULATIONS

In this section I present two separate sets of the data: the Lick indices for the nuclei, $r < 1''$, and the Lick indices for the bulges taken over one-spaxel rings fixed at r_e(bul) for slightly inclined galaxies, $i < 50°$, or at the distance of r_e(bul) from the nuclei along the minor axes for nearly edge-on galaxies. Mean (close to luminosity-weighted) parameters of the stellar populations were calculated in the frame of the evolutionary synthesis models of simple stellar populations (SSP). The SSP-equivalent ages, metallicities, and magnesium-to-iron ratios were determined by comparing Mgb versus Fe5270 and Hβ versus $[\mathrm{MgFe52}] \equiv \sqrt{(\mathrm{Mgb} \times \mathrm{Fe5270})}$; I compared my index measurements to the SSP models by Thomas et al. (2003), which are calculated for a set of the magnesium-to-iron ratios. The results—the Lick indices and the SSP-equivalent ages and metallicities—are given in Tables 1 and 2. The typical internal (statistical) accuracy of the indices in Tables 1 and 2 is around 0.1 Å; subsequently, the internal accuracy of the ages is 0.5 Gyr for young populations, $T < 3$ Gyr, 1 Gyr for intermediate ages, $3 < T < 8$ Gyr, and 3 Gyr for older ones. The accuracy of the metallicities is about 0.1 dex.

The team of the ATLAS-3D survey made its own investigation of the stellar population properties of the same targets (McDermid et al. 2015). However, they considered the stellar population properties within apertures centered on the nuclei, with radii taken at fixed fractions of the *totally measured* (integrated) effective radius: $R_e/8$, $R_e/2$, and R_e. Meanwhile the lenticular galaxies that constitute the dominant part of the ATLAS-3D survey consist of at least *two* large-scale components with different properties and evolution, bulges and disks, having very different ratios of *their own* effective radii. So sometimes the characteristics measured by the team of ATLAS-3D within the $R_e/2$ and R_e apertures relate to the bulges and sometimes to the disks, without specifying their

Table 2
Lick Indices and SSP-equivalent Parameters for the Bulges

Galaxy[a]	r_e(bul), $''$	Its source[b]	Eq. Width of [O III]λ5007	Hβ	Mgb	Fe5270	T, Gyr	$[Z/H]$, dex	[Mg/Fe]
N448	4.7	4	0.10	1.72	3.10	2.54	10	−0.2	+0.1
N502	3.5	8	0.20	1.62	3.79	2.91	8	+0.1	+0.1
N509	2.9	8	0.55	2.08	2.50	2.48	3	−0.1	0.0
N516	2.9	8	0.41	1.83	2.84	2.65	5	−0.1	0.0
N525	3.7	4	0.25	1.96	3.15	2.11	6	−0.2	+0.3
N2577	4.0	4	0	1.55	3.99	2.63	14	−0.1	+0.3
N2698	2.2	4	0.10	1.72	4.53	2.89	8	+0.2	+0.3
N2852	5.2	4	0.61	1.51	3.39	2.02	9	−0.3	+0.4
N2859	4.7	3	0.33	1.51	4.13	2.82	10	+0.1	+0.2
N2880	6.4	1	0.16	1.86	3.35	2.57	7	−0.1	+0.15
N2950	5.1	1	0.50	1.76	3.28	2.57	4	0.0	+0.1
N2962	3.5 ± 0.8	3, 7	0.63	1.22	4.21	2.72	12	0.0	+0.3
N3230	4.2	5	0.13	1.20	4.11	2.64	15	−0.1	+0.3
N3245	3.5 ± 0.2	1, 5	0.15	1.42	3.88	2.65	15	−0.15	+0.2
N3248	4.4	3	1.03	1.84	2.76	2.37	3	−0.05	+0.1
N3301	3.3 ± 0.4	3, 7	0.38	1.88	2.81	2.56	5	−0.2	0.0
N3412	8.1	7	0.22	1.85	3.03	2.50	6	−0.15	+0.1
N3599	3.4	3	1.35	1.88	2.72	2.64	2	+0.1	0.0
N3607	7.8 ± 0.3	1, 5	0.43	1.27	4.04	2.64	15	−0.1	+0.3
N3610	3.9	4	0.37	1.97	3.40	2.57	4	+0.05	+0.15
N3613	7.6	4	0.12	1.67	4.08	2.64	9	0.0	+0.3
N3626	2.5 ± 0.1	3, 5	0.40	2.53	2.43	2.37	2	0.0	0.0
N3630	3.7 ± 0.6	4, 7	0.14	1.66	3.74	2.68	10	−0.1	+0.15
N3665	14.4	1	0.16	1.68	3.49	2.35	10	−0.2	+0.3
N3674	2.9	4	0.41	1.40	3.88	2.53	13	−0.2	+0.3
N3757	2.1	3	0.17	1.78	3.62	2.70	7	0.0	+0.15
N3838	2.1	4	0.34	1.98	3.41	2.52	4	0.0	+0.2
N3941	2.9 ± 0.5	2, 3	0.69	1.50	3.77	2.79	5	+0.1	+0.15
N3945	8.5	1	0.33	1.32	3.99	2.80	14	−0.1	+0.15
N4036	8.9	5	0.47	1.37	3.86	2.64	12	−0.1	+0.2
N4111	3.0	3	0.40	1.68	3.55	2.74	5	+0.1	+0.1
N4124	8.0	4	0.42	2.60	2.62	2.39	1.5	+0.1	0.0
N4179	8.1	4	0.18	1.81	3.48	2.52	7	−0.1	+0.2
N4233	4.6 ± 0.2	4, 5	0.54	1.01	4.06	2.58	15	−0.1	+0.3
N4267	4.4	1	0.12	1.55	4.21	2.65	12	0.0	+0.3
N4324	7.8	3	1.07	1.49	3.06	2.59	4	0.0	0.0
N4340	4.4	2	0.23	1.72	3.33	2.99	7	0.0	0.0
N4342	2.6	6	0.1	1.37	4.69	2.90	15	+0.1	+0.3
N4346	3.8 ± 0.4	3, 4	0.34	1.90	3.38	2.70	4	+0.1	+0.1
N4350	3.0	4	0.12	1.32	4.62	2.87	15	+0.1	+0.3
N4371	7.5	3	0.13	1.61	3.83	2.63	11	−0.1	+0.2
N4377	3.4 ± 0.9	5, 7	0.12	1.65	3.35	2.51	11	−0.2	+0.15
N4417	5.3	4	0.17	1.64	3.48	2.44	11	−0.2	+0.2
N4429	10.7	5	0.13	1.74	4.40	2.62	7	+0.1	+0.3
N4434	4.7	4	0.24	1.59	3.36	2.59	10	−0.15	+0.1
N4442	9.2	3	0.10	1.36	4.23	2.65	15	−0.1	+0.3
N4461	4.4	3	0.19	1.69	3.91	2.77	7	+0.1	+0.15
N4474	3.5	4	0.16	1.92	3.32	2.52	5	−0.1	+0.15
N4476	8.2	6	0.52	2.02	2.12	1.72	5	−0.4	+0.15
N4483	3.7	7	0.17	1.93	3.53	2.50	6	−0.05	+0.2
N4503	9.7	3	0.21	1.60	3.94	2.67	10	0.0	+0.2
N4528	3.7	5	0.16	1.97	2.96	2.19	7	−0.25	+0.2
N4578	10.3 ± 3.9	4, 5	0.42	1.94	3.36	2.49	4	0.0	+0.15
N4596	2.8	2	0.31	1.17	4.23	2.80	15	−0.05	+0.2
N4608	3.3	2	0.15	1.64	3.85	2.69	10	0.0	+0.2
N4623	11.9	4	0.26	2.02	3.00	2.49	4	−0.1	+0.1
N4643	4.2 ± 1.0	2, 3	0.26	1.45	3.86	2.76	12	−0.1	+0.15
N4733	5.7	3	0.25	2.06	2.82	2.51	5	−0.15	0.0
N4754	4.4 ± 1.6	1, 3	0.	1.39	3.93	2.79	15	−0.1	+0.15
N4762	3.1	4	0.24	1.77	4.13	2.82	5	+0.2	+0.2
N5103	1.9	4	0.44	1.64	3.51	2.65	7	−0.1	+0.15
N5342	1.7	4	0.16	1.27	4.01	2.25	15	−0.2	+0.4
N5353	5.4	7	0	1.32	4.82	3.15	15	+0.25	+0.2
N5355	7.4	3	0.40	2.11	2.43	2.22	4	−0.2	0.0

Table 2
(Continued)

Galaxy[a]	r_e(bul), $''$	Its source[b]	Eq. Width of [O III]λ5007	Hβ	Mgb	Fe5270	T, Gyr	$[Z/H]$, dex	[Mg/Fe]
N5358	2.1	4	0.23	1.96	3.13	2.59	4	0.0	+0.1
N5422	6.2 ± 2.0	3, 4	0.53	1.70	3.78	2.32	6	−0.1	+0.4
N5473	2.7 ± 0.1	1, 3	0.	1.73	4.26	2.74	9	+0.1	+0.4
N5485	10.6 ± 1.6	1, 5	0.16	1.67	4.10	2.54	9	0.0	+0.3
N5493	5.9	1	0.14	1.73	2.36	2.17	13	−0.4	0.0
N5507	3.0 ± 0.1	3, 4	0.49	1.21	4.32	2.56	15	−0.1	+0.3
N5574	10.3	3	0.31	2.59	2.69	1.94	2	−0.2	+0.3
N5611	2.1	…	0.18	1.62	3.17	2.32	12	−0.3	+0.2
N5631	6.5	1	0.34	1.60	3.28	2.47	9	−0.15	+0.15
N5687	5.7 ± 1.8	4, 5	0	1.55	3.97	2.75	14	−0.1	+0.2
N5854	4.9	3	0.45	2.46	2.94	2.56	1.5	+0.2	0.0
N5864	2.5	3	0.21	1.85	3.38	2.65	5	0.0	+0.1
N6017	7.6	4	0.455	1.94	2.17	1.88	5	−0.4	0.0
N6149	3.2	4	0.60	1.31	2.98	2.30	15	−0.4	+0.2
N6278	2.9 ± 0.6	3, 4, 5	0.25	1.22	4.60	3.12	15	+0.2	+0.2
N6703	4.2	1	0.22	1.44	3.94	2.99	11	+0.1	+0.1
N7710	3.0	…	0.30	1.26	2.94	2.27	>8	<−0.4	+0.2
N7743	2.7 ± 1.1	1, 3	1.05	1.99	2.59	2.77	2	+0.1	0.0
I560	2.9	4	1.62	2.01	2.56	2.02	2	−0.2	+0.2
U4551	3.4	3	0.42	1.48	3.70	2.58	10	−0.1	+0.2
P28887	3.7	4	0.37	1.21	2.54	1.74	>8	<−0.4	+0.3
P35754	3.1	4	0.78	1.44	2.94	1.99	9	−0.35	+0.3

Notes.
[a] Galaxy ID: N = NGC, U = UGC, P = PGC, I = IC.
[b] The sources of the r_e(bul) are numbered as follows: (1) Laurikainen et al. (2010); (2) Laurikainen et al. (2005); (3) Salo et al. (2015); (4) Krajnovic et al. (2013); (5) Méndez-Abreu et al. (2008); (6) D'Onofrio (2001); (7) Baggett et al. (1998); (8) Il'ina & Sil'chenko (2012).

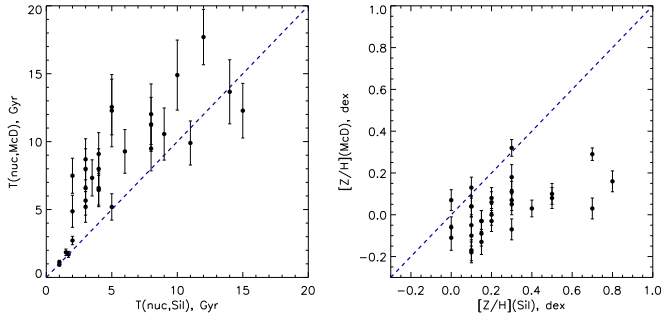

Figure 4. Comparison of the nuclear stellar population parameters—the SSP-equivalent ages and metallicities—derived through the Lick indices in this work with those obtained by McDermid et al. (2015), for the subsample with $R_e/8$ less than 1.5 arcsec.

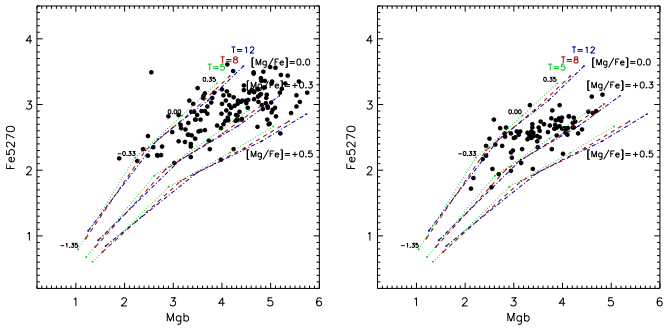

Figure 5. Mgb vs. Fe5270 diagrams for the nuclei (left plot) and for the bulges at one bulge effective radius (right plot). The points are the galaxies of the sample, and the lines refer to the models; the simple stellar population models by Thomas et al. (2003) for three different magnesium-to-iron ratios (0.0, +0.3, and +0.5) and three different ages (5, 8, and 12 Gyr) are plotted as a reference frame. The small symbols along the model curves mark the metallicities of +0.35, 0.00, –0.33, and –1.35, if one takes the symbols from right to left.

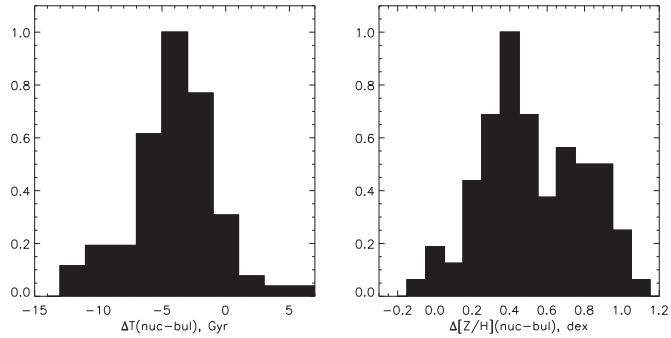

Figure 6. Distributions of the stellar population parameter differences "nucleus minus bulge": (left panel) the age difference between the nuclei and bulges; (right panel) the metallicity difference between the nuclei and bulges. The histograms are normalized to unity at the maximum.

attribution by McDermid et al. (2015). My investigations of the radially resolved properties of stellar populations in S0 galaxies have revealed a quite different evolution of the S0 galaxy constituents—stellar nuclei, bulges, and disks (Sil'chenko 2006, 2008; Sil'chenko et al. 2012)—so I prefer to analyze *separately* the stellar nuclei and the bulges when I operate with the SAURON data. I can compare directly my estimates with the results of McDermid et al. (2015) only in one case, if I take my measurements for the *nuclei* and the measurements by McDermid et al. (2015) for $R_e/8$, after selecting the subsample for comparison by putting a limit on the integrated effective radius presented in Cappellari et al. (2011a): $R_e < 12''$. This limit allows us to consider the $R_e/8$ apertures for the comparison galaxies as being close to the size of the resolved spatial element (seeing) given $R_e/8 < 1''.5$. The comparison of the nuclear stellar population properties is

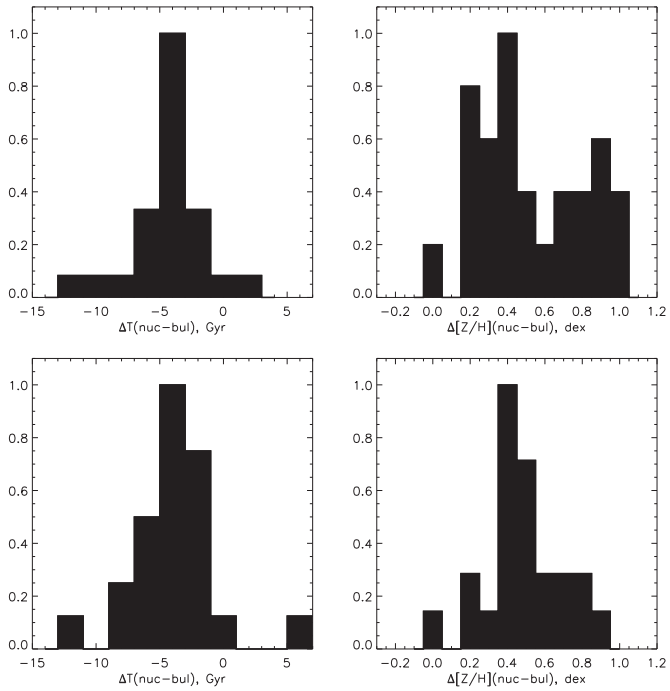

Figure 7. Same as in Figure 6 but with separation according to the environment density: the upper row presents the results for the Virgo S0s, the bottom row for the galaxies within environments sparser than the median one for the whole sample. The data on the environment density are taken from Cappellari et al. (2011b). The histograms are normalized to unity at the maximum.

presented in Figure 4. The age estimates are well correlated, although for intermediate ages, $T = 3$–7 Gyr, a shift by about 4 Gyr can be noted, with the ages by McDermid et al. (2015) looking older. Subsequently, the metallicity estimates are also correlated, but my estimates are higher by some 0.2 dex; three galaxies with $[Z/H] > 0.6$ are strongly off, but such high metallicities are absent in the model set by Thomas et al. (2003) and are perhaps improperly extrapolated. Taking into account the fact that the indices were compared by me and by McDermid et al. (2015) to quite different SSP models, and that the correction of the Hβ indices for the emission was made through quite different approaches, the divergence of the central stellar population parameters obtained so far may be attributed to this fact. The difference in both models and in the Hβ correction for the emission contamination is significant. Concerning the former issue, I use the models by Thomas et al. (2003), which are based on the classical fitting functions for stellar Lick indices from Worthey et al. (1994), with the inserted dependence on abundance ratios from Tripicco & Bell (1995), and on the fuel consumption theorem approach (Renzini & Buzzoni 1986), while McDermid et al. (2015) use the Schiavon (2007) models, which are based on the fitting functions renewed by Schiavon (2007) and on the theoretical isochrone ("conventional") approach. Concerning the index Hβ correction, I use the empirical calibration of the Hβ emission line through the [O III]λ5007 emission line from Trager et al. (2000a), while McDermid et al. (2015) used the approach proposed by the SAURON team (Sarzi et al. 2006), which allows us to derive full emission-line spectra by subtracting the preliminary fitted full spectrum of the stellar populations.

As for the parameters of the stellar populations in the bulges (Table 2), they are obtained not for the whole sample but only for the galaxies whose r_e(bul) are within the field of view of the SAURON, and they also can be resolved with the typical seeing quality of $1\farcs5$; in other words, to study the bulge stellar population properties, I have selected from the ATLAS-3D sample only the S0 galaxies with $1\farcs5 < r_e(\mathrm{bul}) < 15''$. The team of ATLAS-3D had published their own decomposition of the galactic surface-brightness profiles into the sums of a Sérsic bulge and an exponential disk (Krajnovic et al. 2013). But the decomposition was made only for a part of the sample and by analyzing only one-dimensional profiles derived from the SDSS data. They failed to separate two large-scale components in some obvious cases of S0 galaxies with noticeable disks and bulges (NGC 3607, NGC 3665, NGC 4036, NGC 5355). To estimate the bulge effective radii in the small S0 galaxies NGC 5611 and NGC 7710 where the analysis of Krajnovic et al. (2013) has not revealed any disks, I have undertaken my own decomposition of the SDSS one-dimensional surface-brightness profiles and have succeeded in deriving the parameters separately for the bulges and for the disks. To involve more certain data on the bulge's effective radii, I have searched for results of 2D decomposition by considering the decompositions made in near-infrared light as the better ones. Also, other literature sources were searched for galaxies that were not involved in photometric surveys dedicated to the 2D surface-brightness decomposition. Finally, I have collected the bulge's effective radius measurements for the S0 galaxies of the ATLAS-3D sample from eight different sources listed in Table 2. When a galaxy was investigated in several works and the derived r_e(bul) were close, I took the averaged value, which is given in Table 2 with a corresponding estimate of the r_e(bul) scatter. When all the results for r_e(bul) were strongly different, I took the estimates obtained by the 2D near-infrared decomposition from Laurikainen et al. (2010) or from Salo et al. (2015). The adopted values of r_e(bul) are listed in Table 2 with the corresponding references to their sources.

Figures 5–7 demonstrate some statistics on the stellar population properties obtained. The magnesium-to-iron ratios (Figure 5) are mostly between [Mg/Fe] = 0 and [Mg/Fe] = +0.3 both for the nuclei and for the bulges; however, the whole distribution of the bulges in the (Mgb, Fe5270) diagram is shifted to lower metallicities with respect to that of the nuclei. As I noted earlier more than once—see, for example, Sil'chenko et al. (1992) and Sil'chenko (2006, 2008)—the stellar nuclei are chemically and evolutionarily decoupled with respect to the bulges: they are not simply the central points ($R = 0$) of the bulges. In Figure 6 one can see that the nuclei are typically younger and more metal-rich than the bulges. Earlier (Sil'chenko 2008) I estimated the fraction of chemically distinct nuclei in nearby S0s as one-half of the sample; now, with the volume-limited sample of the ATLAS-3D, I increase this estimate to at least 84%. In Figure 6 the age difference distribution has a maximum at –4 Gyr, and the metallicity difference distribution has two peaks, at +0.4 dex and at +0.8 dex. I have divided the whole sample into two subsamples according to the local environment density. The local environment densities for the galaxies of the ATLAS-3D sample have been estimated by Cappellari et al. (2011b), and it is from this paper that I have taken the environment density estimators Σ_{10} for every galaxy. Cappellari et al. (2011b) noted that a condition $\log\Sigma_{10} > 0.4$ separates well the Virgo members from other galaxies, so I have taken two subsamples, with $\log\Sigma_{10} > 0.4$ ("cluster and rich-group members") and

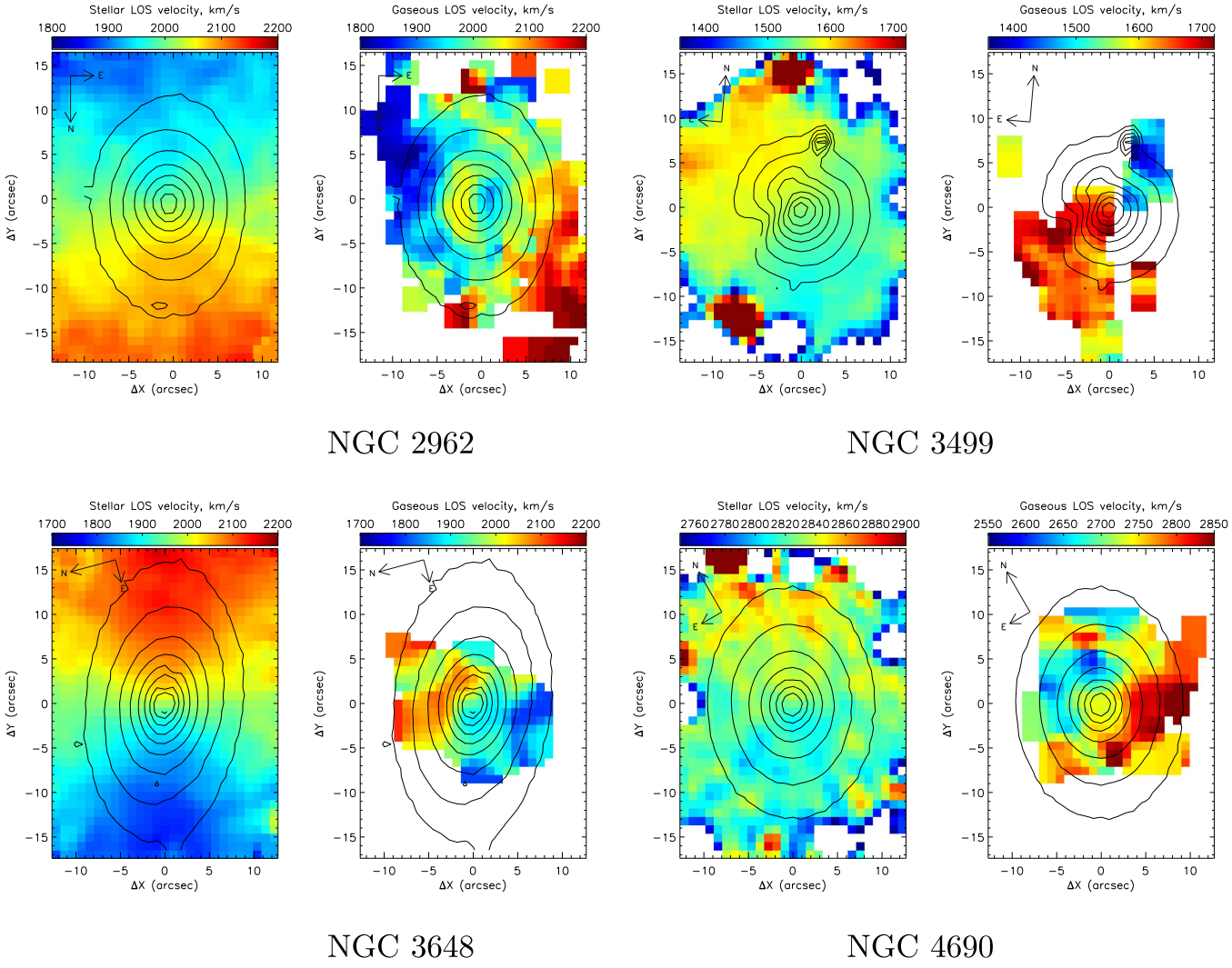

Figure 8. Line-of-sight velocity fields for the stellar (left plot in each pair) and ionized-gas (right plot in each pair) components in four lenticular galaxies, constructed using the SAURON panoramic spectral data. To derive the ionized-gas velocity fields, the measurements of the [O III]λ5007 emission line were used. The green continuum isophotes, $\lambda = 5100$ Å, are overplotted.

Table 3
Orientations of the Rotation Planes for the Stars and Ionized Gas in Five S0 Galaxies

NGC	PA_{kin}(stars), deg	i_{kin}(stars), deg	Radius (gas), arcsec	PA_{kin}(gas), deg	i_{kin}(gas), deg	$\Delta\psi$, deg
2962	7 ± 1.5	47 ± 3	6–11	80 ± 3	63.5 ± 2.5	60 or 83.5
2962	7 ± 1.5	47 ± 3	13–18	51.5 ± 1.5	78 ± 1	50 or 111
3499	38 ± 4	48 ± 8	5–11	133 ± 3	62 ± 5.5	75 or 68
3648	253 ± 3	54 ± 7	1–4	282 ± 4	66 ± 3	28 or 114
3648	253 ± 3	54 ± 7	5–8	332 ± 3	67 ± 1	68 or 85
4690	332 ± 7	18 ± 10	3–6	169 ± 2	71 ± 4	88 or 54
4690	332 ± 7	18 ± 10	7–8	225 ± 8	65 ± 13	71 or 61
5507	63 ± 3	64 ± 5	2–6	138 ± 2	64 ± 4	66 or 91

with $\log \Sigma_{10} < -0.65$ ("isolated galaxies"), to plot the distributions of the age and metallicity differences betwen the nuclei and the bulges in Figure 7. It becomes clear (Figure 7) that the second peak in the metallicity difference distribution is due completely to the Virgo members, while the broadening of the age difference distribution is produced by the galaxies in low-density environments. An evident dependence of the evolution paths of S0 galaxies on the environment density is implied by these results.

5. NEWLY DISCOVERED INNER POLAR DISKS, AND STATISTICS OF INNER POLAR DISKS OVER THE VOLUME-LIMITED SAMPLE OF NEARBY S0 GALAXIES

In the ATLAS-3D volume-limited sample of nearby S0s, I have found seven new cases of polar gas rotation. In five of them the gas velocity fields have appeared to be extended enough, at least 5–10 spaxels from the center, and the main stellar disks are not strictly edge-on, to give a possibility to

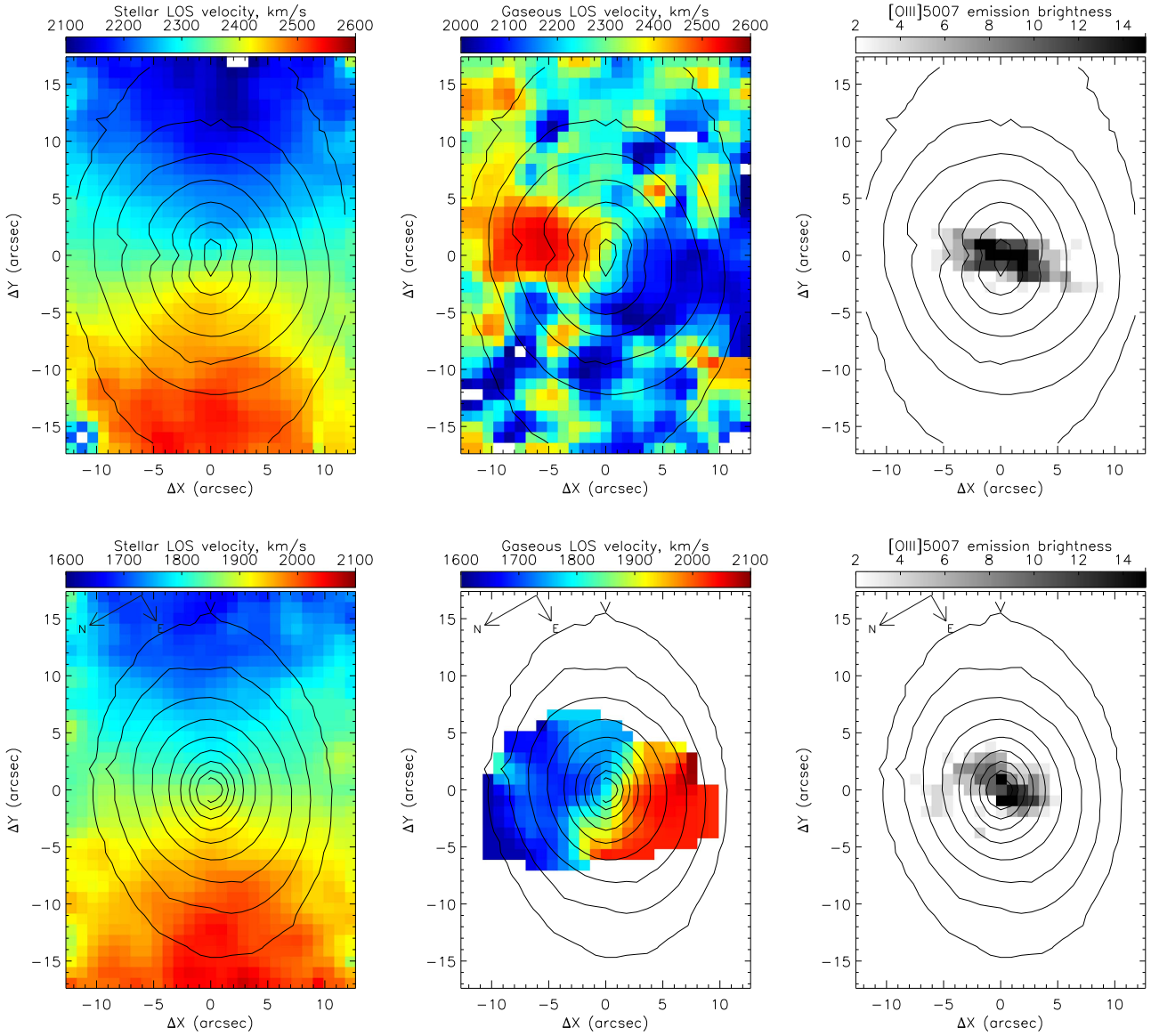

Figure 9. Stellar and gaseous velocity fields and the [O III] emission-line intensity distributions in NGC 4233 (top row) and NGC 5507 (bottom row). The green continuum isophotes, $\lambda = 5100$ Å, are overplotted.

apply to them the tilted-ring DETKA software. The results, namely, the orientation angles of the rotation planes for the stellar and for the gaseous components as well as the estimated mutual inclinations of the gaseous and stellar rotation planes, are presented in the Table 3. In three galaxies—NGC 2962, NGC 3648, and NGC 4690—I see warps of the inner gaseous disks or even several nested gaseous rings with slightly different orientations; for these galaxies I give the results in two separate radius ranges.

Some examples of the velocity fields for the stellar and gaseous components in the galaxies with inner polar disks are shown in Figure 8. As a confirmation, or visual signatures of the inner polar disk presence, especially in the cases when the gaseous disks are seen edge-on, I use also the maps of the emission-line intensities (as illustration, the [O III]λ5007 maps for NGC 5507 and NGC 4233 are presented in Figure 9) and the color maps constructed by using the SDSS archive (DR9) data; the examples for UGC 9519 and NGC 3499 are given in Figure 10. I note here that the polar inner disks in NGC 4233 and UGC 9519 were reported earlier, by Sil'chenko & Afanasiev (2004) for the former and by Katkov et al. (2014a) for the latter galaxy. As for UGC 9519, the ATLAS-3D team also reported the external source of the misaligned cold neutral gas for this galaxy (Davis et al. 2011).

Below some details of the gas distributions and motions in individual galaxies discussed here are specified.

NGC 1121. The circumnuclear gaseous subsystem of this galaxy seen in the [O III]λ5007 emission line is too compact to be analyzed with the DETKA software. However, it is the case where the stellar disk of the galaxy is seen edge-on, and the centrally concentrated gas evidently rotates off the main galactic plane (Figure 11, upper plots).

NGC 2962. This bona fide S0 galaxy is however very gas-rich: Grossi et al. (2009) report some 10^9 solar masses of neutral hydrogen in NGC 2962 distributed regularly in an extended disk cospatial with the stellar one. But in the center (Figure 8, upper left), we see several nested gaseous subsystems with decoupled rotation: though all kinematical

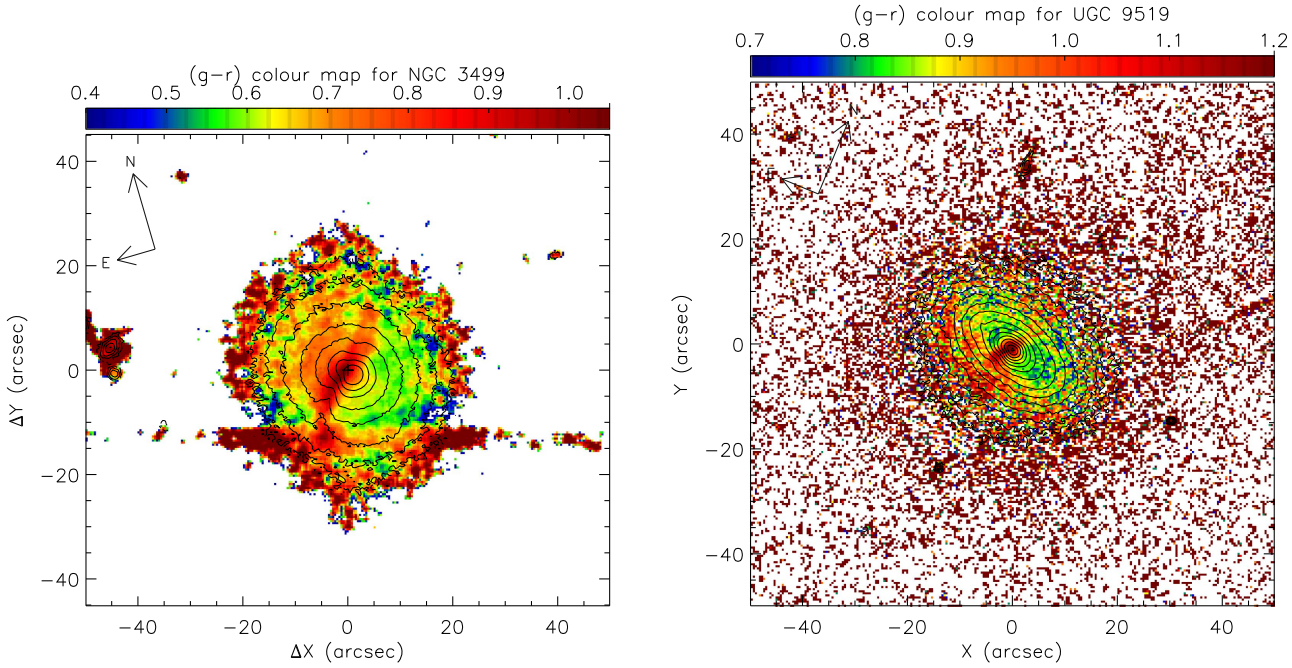

Figure 10. Color maps for NGC 3499 (left) and UGC 9519 (right) derived from the SDSS/DR9 data.

major axes are roughly perpendicular to the isophote major axis (by some 80°), the very inner ionized gas, at $R < 4''$, counterrotates with respect to the more outer gas. At $R = 5''$–$18''$ the gas rotation plane is strongly inclined, but not strictly polar, and undergoes a smooth warp along the radius.

NGC 3499. This is an isolated (Karachentsev et al. 2011), small, close to face-on S0/a galaxy. Its HI content is rather modest but detectable: 7×10^7 solar masses according to the Green Bank Telescope integrated data (Wei et al. 2010). Wei et al. (2010) describe the neutral hydrogen distribution in NGC 3499 as a regularly rotating extended disk, with a rotation velocity of 119 sin i km s^{-1}. We see orthogonality of the kinematical major axes of the stellar and ionized-gas components in the center of the galaxy ($PA_* = 38° \pm 4°$ versus $PA_{gas} = 133° \pm 3°$, Figure 8, upper right), and also a dust lane aligned in PA = 132°, just as the kinematical major axis of the ionized gas (Figure 10) but projected off the nucleus, so the central gaseous disk is not strictly edge-on.

NGC 3648. This galaxy lacks HI, according to Serra et al. (2012), so we can suggest a compact circumnuclear ionized-gas disk, warped and becoming nearly polar at $R > 5''$ (Table 3).

NGC 4026. This galaxy is strictly edge-on. In the central part the gaseous component looks like a disk seen edge-on, inclined by some 50° to the main galactic plane. Farther from the center, the gaseous disk warps and lies in the galactic plane. The HI map presented by Serra et al. (2012) demonstrates a long, gas-rich filament entering the disk of the galaxy just near the center at a right angle. Perhaps we see here the nearly polar gas accretion through the cosmological filament and strong plane precession over the outer parts of the extended gaseous disk.

NGC 4690. This galaxy lacks detections both of neutral (Bettoni et al. 2003) and molecular gas (Young et al. 2011). In our maps (Figure 8, bottom right) we see a sort of ionized-gas ring starting at a radius of $R \approx 2''$, extending toward $R \approx 8''$, with a possible warp at the edge, with the PA_{kin}(gas) changing by some 55° over the radius range of 3 arcsec. The outer, $R = 7''$–$8''$, orientations of the disk lines of nodes, PA_{kin}(stars) and PA_{kin}(gas), are strictly orthogonal.

NGC 5507. This is also the galaxy where we can suggest a source of the polar gas accretion: it has a luminous late-type neighbor, NGC 5506, at 25 kpc from it. The circumnuclear ionized gaseous disk of NGC 5507 seen in [O III]λ5007 is edge-on and roughly west–east elongated (Figure 9), just as NGC 5506 as a whole. However, the kinematical major axis of this disk is oriented in PA = 138° and so is revealing radial gas motions, most probably inflow: the superposition of the circular rotation having the disk line of nodes aligned in PA ≈ 90° with pure radial motions of comparable velocity amplitude would result in a kinematical major axis turned by 45°.

Besides these seven S0 galaxies with polar inner disks found so far in the ATLAS-3D sample, we can refer also to the inner polar disks in UGC 9519 implied by the polar dust lane (Figure 10, right) and gas decoupled kinematics (Katkov et al. 2014a), and in the strongly emissive NGC 4684 where the stellar disk is seen edge-on and the circumnuclear gas is aligned at the direct angle with respect to the main galactic body (Davis et al. 2011). When we expand the present sample of 143 S0s toward the full sample of the ATLAS-3D survey including early observations in the frame of the SAURON project (Bacon et al. 2001), we obtain 200 lenticular galaxies in the local volume limited by $D < 42$ Mpc; according to Cappellari et al. (2011a), this sample is complete over the galaxy luminosities exceeding $M_K < -21.5$. By adding to the nine inner polar disks mentioned above the galaxies listed by Moiseev (2012), we claim the detection of 21 inner polar disks among the full sample of 200 nearby lenticulars. Therefore, the frequency of strongly inclined inner gaseous disks in the nearby S0s is about 10%. We must note that this is much higher than the incidence of large-scale polar rings, which is <1% (Moiseev et al. 2011; Reshetnikov et al. 2011).

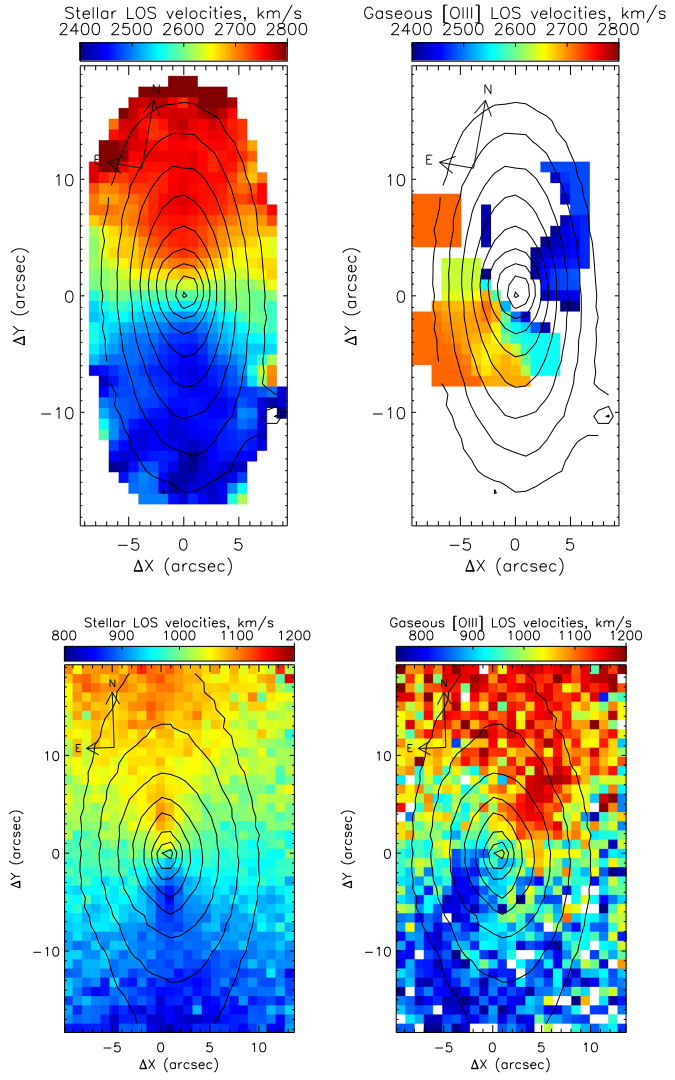

Figure 11. Stellar and gaseous LOS velocity fields of two edge-on galaxies: NGC 1121 (upper plots) and NGC 4026 (lower plots). In the central parts the gaseous disks are inclined to the main galactic planes by some 50°.

6. DO THE INNER POLAR DISK HOSTS DIFFER FROM OTHERS?

Though many lenticular galaxies contain cold gas (Welch & Sage 2003; Sage & Welch 2006; Welch et al. 2010; Davis et al. 2011; Young et al. 2014), only for gaseous subsystems with decoupled kinematics there exists the commonly accepted view that they have been accreted from outside. Among the gaseous subsystems with decoupled kinematics, the polar disks are thought to appear in a host galaxy by capturing the gas with orthogonal orbital momentum from somewhere outside; see, for example, Bournaud & Combes (2003) and Brook et al. (2008). Moreover, polar gas, though accreted from outside, is considered to be dynamically stable and to inhabit long-lived orbits in S0 galaxies (Bournaud & Combes 2003; Mapelli et al. 2015). While the outer gas captured in the main galactic plane of a host galaxy must sink by spiraling into the center on a timescale of 1 Gyr (Walker et al. 1996) and is expected to feed the central star-formation burst with subsequent rejuvenation of the nuclear stellar population, the polar gas may remain off the nucleus and avoid affecting the nuclear stellar population properties.

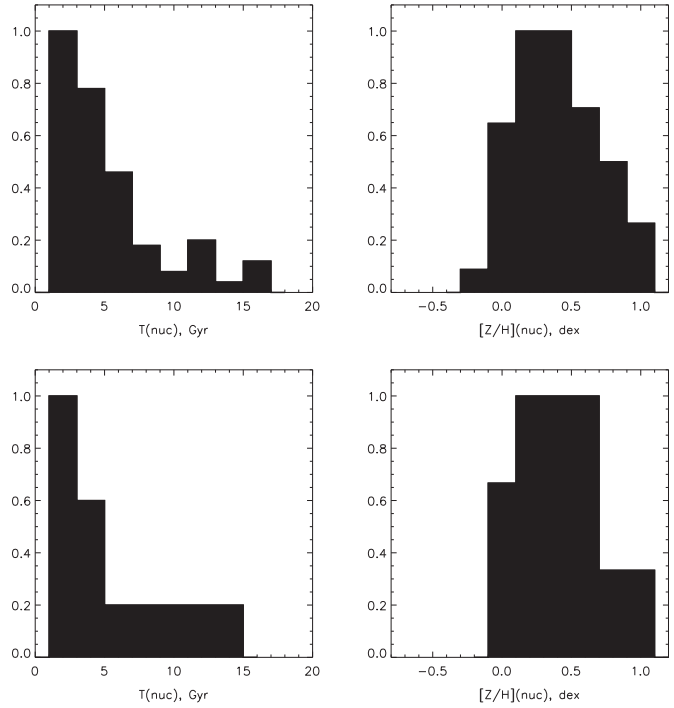

Figure 12. Distributions of the SSP-equivalent characteristics of the nuclear stellar populations in the large sample of the ATLAS-3D S0s (top row) and in the inner polar disk hosts (bottom row). The age distributions are to the left and the metallicity distributions to the right.

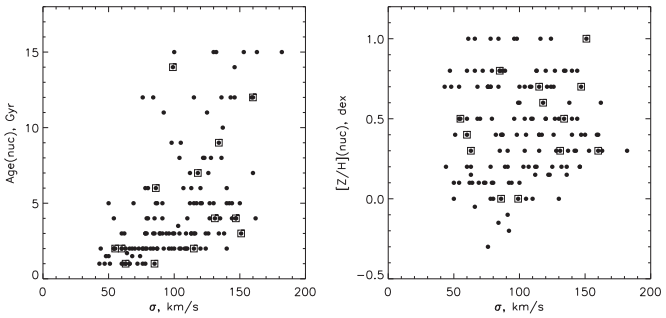

Figure 13. Correlations of the nuclear stellar population SSP-equivalent ages (left) and metallicities (right) with the central stellar velocity dispersion. The points corresponding to the inner polar disk hosts are marked with open squares.

Having the complete sample of nearby S0s, among which 10% of the galaxies possess inner polar disks, I can compare the properties of the nuclear stellar populations in the inner polar disk hosts with the mean characteristics of the whole population of nearby S0s. Figure 12 shows the distributions of the SSP-equivalent ages and metallicities of the nuclear stellar populations for the whole sample of 143 S0s and separately for the hosts of the inner polar disks—seven new ones and six known previously (Moiseev 2012). The total nuclear age distribution is very specific, with most galaxies concentrating around the nucleus age of $T = 2$–3 Gyr, while the minority have old nuclei. The shape of the nucleus-age distribution for the galaxies with the inner polar disks repeats the general distribution perfectly (the Kolmogorov–Smirnov criterium is equal to 0.41): we cannot say that the nuclei in the hosts of the inner polar disks are older or younger on average. Most nuclei, eight of 13, in the S0s with inner polar disks are rather young, 1–4 Gyr old. Their range of metallicity, $[Z/H] \geqslant 0.0$,

fits perfectly the total distribution of the nuclear stellar population metallicities in the nearby S0s. We can conclude that the evolution of the central parts of the inner polar disk hosts is quite the same as that of the whole population of S0s, mainly with a secondary nuclear star-formation burst at a redshift of $z < 0.5$ (<5 Gyr ago).

Figure 13 presents the relations between the age or metallicity of the nuclear stellar populations and the stellar velocity dispersion averaged over apertures of $6\farcs5$ and so characterizing the bulge masses. The hosts of the inner polar disks are marked with open squares to separate out their positions among the total distributions. In general, early-type galaxies reveal tight correlations between these characteristics: $[Z/H]$ correlates with σ_* for the cluster early-type galaxies (Trager et al. 2000b), while the ages correlate with σ_* for samples of field galaxies starting from group environments (Trager et al. 2000b; Caldwell et al. 2003; Howell 2005). In our data we see that the hosts of the inner polar disks spreading over the full range of σ_* participate in the total relations, which resemble in general the relations for field early-type galaxies. However, the relation of age versus σ_* in Figure 13 is unexpectedly curious: only young nuclei, $T < 7$ Gyr, reveal the tight correlation of their ages with the masses of the bulges. Among the old nuclei, no connection between the ages of the nuclear stellar populations and the masses of the bulges can be found. The nuclei of the hosts of the inner polar disks share this behavior: 10 younger nuclei distributed between $\sigma_* = 50$ and 150 km s^{-1} demonstrate good correlation of their ages versus σ_*, while among the hosts of three older nuclei the oldest one is the less massive: it has only $\sigma_* = 100$ km s^{-1}.

7. CONCLUSIONS

I have inspected the central stellar population properties and also the gaseous and stellar kinematics of the volume-limited sample of nearby S0 galaxies observed with the IFU SAURON in the frame of the ATLAS-3D project. I have found seven new cases of nearly polar rotation of the circumnuclear warm-gas disks with respect to the stars. Together with these new findings, I report the presence of 21 inner polar disks among the complete sample of 200 nearby S0s. This means that the frequency of the inner polar gas rotation is about 10% for the early-type disk galaxies in the local universe, which is much higher than the incidence of large-scale polar rings at <1% (Moiseev et al. 2011). Perhaps this difference reflects the natural difference between frequencies of minor and major mergers. To my surprise, the properties of the nuclear stellar populations of the inner polar disk hosts are strictly the same as those of the whole sample of nearby S0s. In particular, the age distributions are quite similar, with the most galaxies concentrated around the value of the nuclear stellar age of 1–4 Gyr. This means that despite the proposed stability of polar orbits, the gas reached the very centers and provoked recent star-formation bursts in the nuclei of the inner polar disk hosts, as it took place in the majority of S0 galaxies. It remains to be understood if the S0 galaxies suffered multiple gas-accretion events, with only a single one of them from a polar orbit.

The present study makes use of data obtained from the Isaac Newton Group Archive, which is maintained as a part of the CASU Astronomical Data Centre at the Institute of Astronomy, Cambridge, UK. This research is also partly based on SDSS data. Funding for the Sloan Digital Sky Survey (SDSS) and SDSS-II has been provided by the Alfred P. Sloan Foundation, the Participating Institutions, the National Science Foundation, the U.S. Department of Energy, the National Aeronautics and Space Administration, the Japanese Monbukagakusho, the Max Planck Society, and the Higher Education Funding Council for England. The SDSS Web site is http://www.sdss3.org/. The whole work was supported by the Russian Science Foundation (project number 14-22-00041).

REFERENCES

Afanasiev, V. L., & Moiseev, A. V. 2011, BaltA, 20, 363
Bacon, R., Copin, Y., Monnet, G., et al. 2001, MNRAS, 326, 23
Baggett, W. E., Baggett, S. M., & Anderson, K. S. J. 1998, AJ, 116, 1626
Baldwin, J. A., Phillips, M. M., & Terlevich, R. 1981, PASP, 93, 5
Bettoni, D., Fasano, G., & Galletta, G. 1990, AJ, 99, 1789
Bettoni, D., Galletta, G., & Garcia-Burillo, S. 2003, A&A, 405, 5
Bigiel, F., Leroy, A. K., Walter, F., et al. 2011, ApJL, 730, L13
Bournaud, F., & Combes, F. 2003, A&A, 401, 817
Brook, C. B., Governato, F., Quinn, T., et al. 2008, ApJ, 689, 678
Burgess, A. 1958, MNRAS, 118, 477
Caldwell, N., Rose, J. A., & Concannon, K. D. 2003, AJ, 125, 2891
Cappellari, M., Emsellem, E., Krajnovic, D., et al. 2011a, MNRAS, 413, 813
Cappellari, M., Emsellem, E., Krajnovic, D., et al. 2011b, MNRAS, 416, 1680
Chiosi, C. 1980, A&A, 83, 206
Corsini, E. M., Pizzella, A., Coccato, L., & Bertola, F. 2003, A&A, 408, 873
Dalcanton, J. J. 2007, ApJ, 658, 941
Davis, T. A., Alatalo, K., Sarzi, M., et al. 2011, MNRAS, 417, 882
de Zeeuw, P. T., Bureau, M., Emsellem, E., et al. 2002, MNRAS, 329, 513
D'Onofrio, M. 2001, MNRAS, 326, 1517
Fisher, D., Franx, M., & Illingworth, G. 1996, ApJ, 459, 110
Grossi, M., di Serego Alighieri, S., Giovanardi, C., et al. 2009, A&A, 498, 407
Howell, J. H. 2005, AJ, 130, 2065
Il'ina, M. A., & Sil'chenko, O. K. 2012, ARep, 56, 578
Karachentsev, I. D., Makarov, D. I., Karachentseva, V. E., & Melnyk, O. V. 2011, AstBu, 66, 1
Katkov, I. Yu., Moiseev, A. V., & Sil'chenko, O. K. 2011, ApJ, 740, Aid83
Katkov, I. Yu., Sil'chenko, O. K., & Afanasiev, V. L. 2014a, MNRAS, 438, 2798
Katkov, I. Yu., Sil'chenko, O. K., & Afanasiev, V. L. 2014b, AstBu, 69, 121
Krajnovic, D., Alatalo, K., Blitz, L., et al. 2013, MNRAS, 432, 1768
Krajnovic, D., Emsellem, E., Cappellari, M., et al. 2011, MNRAS, 414, 2923
Kuntschner, H., Emsellem, E., Bacon, R., et al. 2006, MNRAS, 369, 497
Laurikainen, E., Salo, H., & Buta, R. 2005, MNRAS, 362, 1319
Laurikainen, E., Salo, H., Buta, R., Knapen, J. H., & Comerón, S. 2010, MNRAS, 405, 1089
Mapelli, M., Rampazzo, R., & Marino, A. 2015, A&A, 575, A16
McDermid, R. M., Alatalo, K., Blitz, L., et al. 2015, MNRAS, 448, 3484
Méndez-Abreu, J., Aguerri, J. A. L., Corsini, E. M., & Simonneau, E. 2008, A&A, 478, 353
Moiseev, A. V. 2012, AstBu, 67, 147
Moiseev, A. V., Smirnova, K. I., Smirnova, A. A., & Reshetnikov, V. P. 2011, MNRAS, 418, 244
Moiseev, A. V., Valdés, J. R., & Chavushyan, V. H. 2004, A&A, 421, 433
Naim, A., Lahav, O., Buta, R. J., et al. 1995, MNRAS, 274, 1107
Pilyugin, L. S., Vílchez, J. M., & Contini, T. 2004, A&A, 425, 849
Pizzella, A., Corsini, E. M., Vega Beltrán, J. C., & Bertola, F. 2004, A&A, 424, 447
Proshina, I. S., Kniazev, A. Yu., & Sil'chenko, O. K. 2016, AstL, accepted
Renzini, A., & Buzzoni, A. 1986, in Spectral Evolution of Galaxies, ed. C. Chiosi & A. Renzini (Dordrecht: Reidel), 195
Reshetnikov, V. P., Faúndez-Abans, M., & de Oliveira-Abans, M. 2011, AstL, 37, 171
Sage, L. J., & Welch, G. A. 2006, ApJ, 644, 850
Salo, H., Laurikainen, E., Laine, J., et al. 2015, ApJS, 219, 4
Sarzi, M., Falcón-Barroso, J., Davies, R. L., et al. 2006, MNRAS, 366, 1151
Schiavon, R. P. 2007, ApJS, 171, 146
Serra, P., Oosterloo, T., Morganti, R., et al. 2012, MNRAS, 422, 1835
Sil'chenko, O. K. 2005, AstL, 31, 227
Sil'chenko, O. K. 2006, ApJ, 641, 229
Sil'chenko, O. K. 2008, in IAU Symp. 245, Formation and Evolution of Galaxy Bulges, ed. M. Bureau, E. Athanassoula, & B. Barbuy (Cambridge: Cambridge Univ. Press), 277
Sil'chenko, O. K. 2013, MmSAI Supplement, 25, 93

Sil'chenko, O. K., & Afanasiev, V. L. 2000, A&A, 364, 479
Sil'chenko, O. K., & Afanasiev, V. L. 2004, AJ, 127, 2641
Sil'chenko, O. K., Afanasiev, V. L., & Vlasyuk, V. V. 1992, AZh, 69, 1121
Sil'chenko, O. K., & Moiseev, A. V. 2006, AJ, 131, 1336
Sil'chenko, O. K., Moiseev, A. V., & Shulga, A. P. 2010, AJ, 140, 1462
Sil'chenko, O. K., Proshina, I. S., Shulga, A. P., & Koposov, S. E. 2012, MNRAS, 427, 790
Sil'chenko, O. K., Vlasyuk, V. V., & Burenkov, A. N. 1997, A&A, 326, 941
Stasinska, G., & Sodré, I., Jr. 2001, A&A, 374, 919
Thomas, D., Maraston, C., & Bender, R. 2003, MNRAS, 339, 897
Tosi, M. 1988, A&A, 197, 47
Trager, S. C., Faber, S. M., Worthey, G., & Gonzàlez, J. J. 2000a, AJ, 119, 1645
Trager, S. C., Faber, S. M., Worthey, G., & Gonzàlez, J. J. 2000b, AJ, 120, 165
Tripicco, M. J., & Bell, R. A. 1995, AJ, 110, 3035
Walker, I. R., Mihos, J. C, & Hernquist, L 1996, ApJ, 460, 121
Wei, L. H., Kannappan, S. J., Vogel, S. N., & Baker, A. J. 2010, ApJ, 708, 841
Welch, G. A., & Sage, L. J. 2003, ApJ, 584, 260
Welch, G. A., Sage, L. J., & Young, L. M. 2010, ApJ, 725, 100
Worthey, G., Faber, S. M., González, J. J., & Burstein, D. 1994, ApJS, 94, 687
Young, L. M., Bureau, M., Davis, T. A., et al. 2011, MNRAS, 414, 940
Young, L. M., Scott, N., Serra, P., et al. 2014, MNRAS, 444, 3408